ACS Photonics

pubs.acs.org/journal/apchd5

Article

Total Reflection-Induced Efficiency Enhancement of the Spin Hall Effect of Light

Minkyung Kim,[#] Dasol Lee,[#] Thi Hai-Yen Nguyen, Hee-Jo Lee, Gangil Byun, and Junsuk Rho*

Cite This: https://doi.org/10.1021/acsphotonics.1c00727

Read Online

ACCESS | Metrics & More | Article Recommendations | Supporting Information

ABSTRACT: The spin Hall effect of light (SHEL) refers to the spin-dependent and transverse splitting of oblique incidence that occurs in both refraction and reflection. Enhancement of the SHEL is generally accompanied by a degradation in the efficiency. Recently, an anisotropic metamaterial has been proposed to attain a large SHEL with near-unity efficiency, but is limited to a horizontally polarized incidence. Here, a new approach to achieve a large SHEL and high efficiency simultaneously for arbitrarily polarized incidence is proposed by exploiting total external and internal reflection. The total reflection at the interface of a dense-to-sparse medium yields a theoretical maximum of the shift that is allowed for a unity efficiency. The SHEL can be further enhanced by increasing the refractive index contrast. Furthermore, we suggest a three-dimensional isotropic metamaterial that is designed to have an index below unity as a platform to experimentally demonstrate the SHEL with high efficiency. Our work will find wide applications in spin-dependent photonic devices.

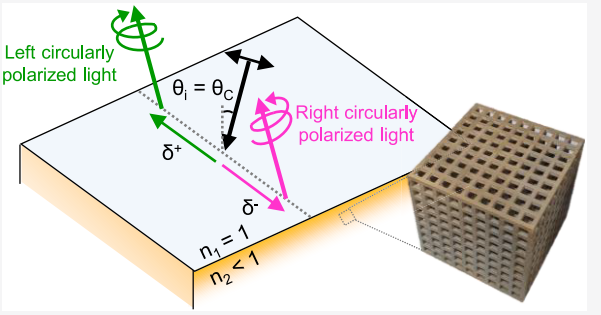

KEYWORDS: *optical spin Hall effect, photonic spin Hall effect, total reflection, high efficiency, index-near-zero metamaterial, ultralow-index metamaterial, microwave*

The vectorial characteristic of light brings out a notion of polarization degree of freedom that is locked to the momentum of light.[1] The coupling of the polarization and momentum can be explained by the transversality of light.[2] This spin−orbit coupling has spawned many interesting phenomena including spin-to-orbital angular momentum conversion,[3] spin-dependent beam shaping,[4] transverse spin,[5] and spin-dependent control of surface waves.[6] Spin Hall effect of light (SHEL) is yet another interesting phenomenon that has its origin in the spin−orbit interaction. The SHEL refers to a spin-dependent and transverse displacement of an obliquely injected beam at an optical interface.[7−10] When a linearly polarized incidence undergoes refraction or reflection, the incidence is split into two circularly polarized light with opposite handedness. This spin-dependent spatial splitting originates from the Berry curvature and correspondingly the Berry phase that has the opposite signs for two circularly polarized beams.[10−12] The amount of the displacement of the refracted or reflected beam, which is also often called a shift, is determined by the Fresnel coefficients of two linear polarizations and the incident angle.[8,13] As the amount of the shift varies sensitively to the geometrical and optical parameters of the interface, the SHEL has been proposed as tools for high precision metrology to measure the geometrical fluctuation of nanostructures,[14] optical conductivity,[15] magnetic properties,[16,17] ion concentration,[18] and so on.[19−22]

Because of weak spin−orbit coupling, the SHEL is generally weak, as manifested by a deep-subwavelength scale of the shift.[8] To enhance the shift by up to an order of wavelength, several approaches have been proposed by using anisotropic materials,[9,23,24] birefriengent materials,[25] and metamaterials/metasurfaces,[26−32] or under specific circumstances.[13,33−38] However, the enhancement of the SHEL in general accompanies attenuation of efficiency. The principles of the enhanced SHEL in many previous proposals lie on a vanishing Fresnel coefficient,[13,33−35] which in turn degrades the efficiency of the whole phenomenon. Recently, the large SHEL with high efficiency has been demonstrated in the microwave regime for horizontal polarization by using an anisotropic impedance mismatching.[39] However, an approach toward the large SHEL and high efficiency for both horizontal and vertical polarizations or general polarization has yet been reported.

Here, we present a new route to achieve the large SHEL and high efficiency simultaneously for any incident polarization

Received: May 17, 2021

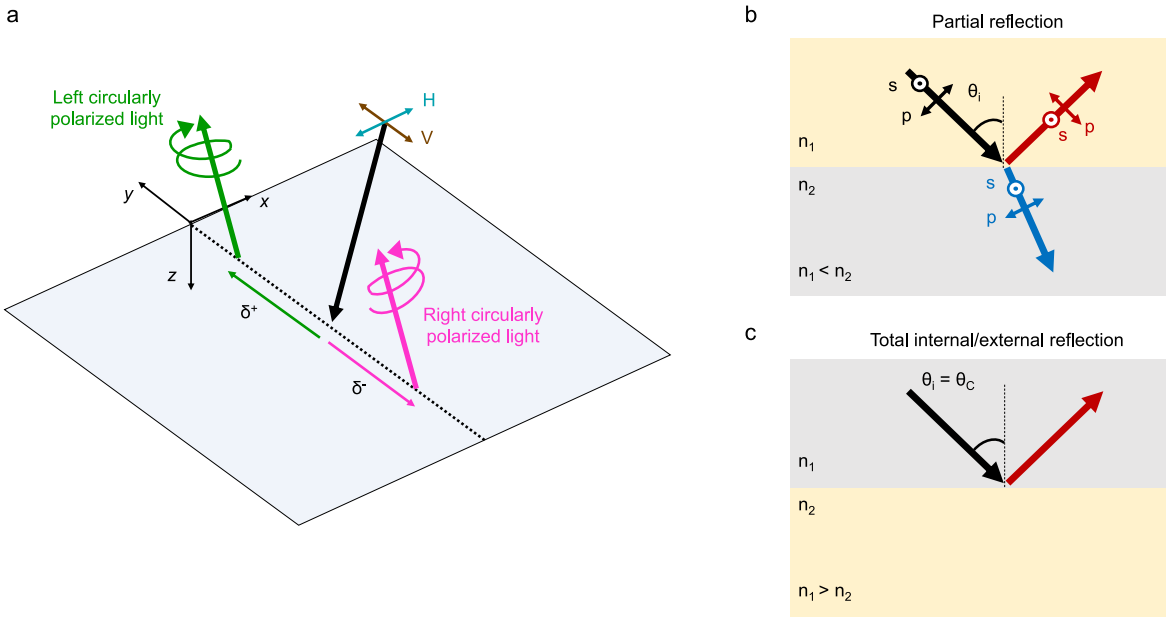

Figure 1. Schematics of SHEL and reflections. (a) Schematic of the reflection type SHEL. (b, c) Schematics of (b) partial and (c) total reflections. Yellow and gray indicate sparser and denser media, respectively.

using total reflection. We demonstrate that total internal and external reflection occurring at an interface of dense-to-sparse medium yields a SHEL that reaches a theoretical maximum of the shift along with a unity efficiency at a critical angle. The large SHEL is determined by the refractive index ratio of the two media and can be further enhanced by increasing the index contrast. Furthermore, we suggest an experimental scheme by using a three-dimensional (3D) isotropic metamaterial that is designed to have an index below unity. The large SHEL with high efficiency under arbitrary polarizations will enable highly efficient devices with spin-selective functionalities and a larger degree of freedom.

RESULTS

Principle. An incidence that has a finite beam waist experiences a spin-dependent shift when it is reflected at an optical interface (Figure 1a). The amount of the shift δ can be obtained as[13]

$$\delta_H^{\pm}/\lambda = \mp\frac{\cot\theta_i}{2\pi}\mathrm{Re}\left(1+\frac{r_s}{r_p}\right),$$
$$\delta_V^{\pm}/\lambda = \mp\frac{\cot\theta_i}{2\pi}\mathrm{Re}\left(1+\frac{r_p}{r_s}\right) \quad (1)$$

when the beam waist w_0 is sufficiently large to satisfy $(2\pi w_0/\lambda)^2 \gg \cot^2\theta_i$. Here, subscripts H and V indicate horizontal and vertical polarization, respectively; superscripts + and − represent left and right circularly polarized light, respectively; λ is a wavelength of the incident beam; θ_i is an incident angle; r_s and r_p are Fresnel reflection coefficients of s and p polarizations. The efficiency of the SHEL is determined by the reflectance as[39]

$$\epsilon_H = |r_p|^2,$$
$$\epsilon_V = |r_s|^2 \quad (2)$$

To search an optimal case that has a large SHEL with high efficiency, we consider reflections at an interface between two media that have constant refractive indices n_1 and n_2 under a lossless assumption ($\{n_1, n_2\} \in \mathbb{R}$), as shown in Figure 1b,c. Light propagating in a medium 1 with n_1 impinges onto a medium 2 with n_2. If $n_1 < n_2$, partial reflection occurs, in which only a fraction of incident light is reflected while the remaining is transmitted (Figure 1b). When the incident angle is equal to a Brewster angle ($\theta_B = \tan^{-1}(n_2/n_1)$), the reflected beam is polarized perpendicularly to the incident plane regardless of the incident polarization. In other words, p-polarized incidence cannot be reflected ($r_p = 0$), while s polarization has a finite reflection coefficient. This vanishing r_p is a key contribution of the gigantic SHEL near θ_B by making $\delta_H^{\pm}$ diverge[13,33−35] (eq 1). However, the vanishing r_p also gives rise to extremely low efficiency ($\epsilon_H \approx 0$), as indicated by eq 2. Therefore, enhancement of the SHEL by reducing Fresnel coefficients in the denominator causes a critical restriction that the large shift and high efficiency cannot be achieved simultaneously.

Recently, the large SHEL with high efficiency has been proposed and realized for horizontally polarized incidence by exploiting an anisotropic impedance mismatching.[39] The large SHEL that has high efficiency can also be realized by a radically different approach using total internal and external reflections. If an incident angle exceeds a critical angle ($\theta_C = \sin^{-1}(n_2/n_1)$), a wave propagating from a medium to a sparser medium ($n_2 < n_1$) is totally reflected for both s and p polarizations (Figure 1c). In other words, $|r_s| = |r_p| = 1$ and, consequently, $\epsilon_H = \epsilon_V = 1$ at $\theta_i > \theta_C$. This total reflection is attributed to the absence of real solutions of the transmitted angle according to Snell's law and is called a total internal reflection if the index of the sparser medium is unity ($n_1 > n_2 = 1$) and a total external reflection if the denser medium has a unity index ($n_2 < n_1 = 1$). In particular, when an incidence is injected at $\theta_i = \theta_C$, r_s and r_p have a zero phase difference, which leads to a shift of

$$\delta_H^{\pm}/\lambda = \delta_V^{\pm}/\lambda = \mp\frac{\cot\theta_C}{\pi} \quad (3)$$

https://doi.org/10.1021/acsphotonics.1c00727
ACS Photonics XXXX, XXX, XXX−XXX

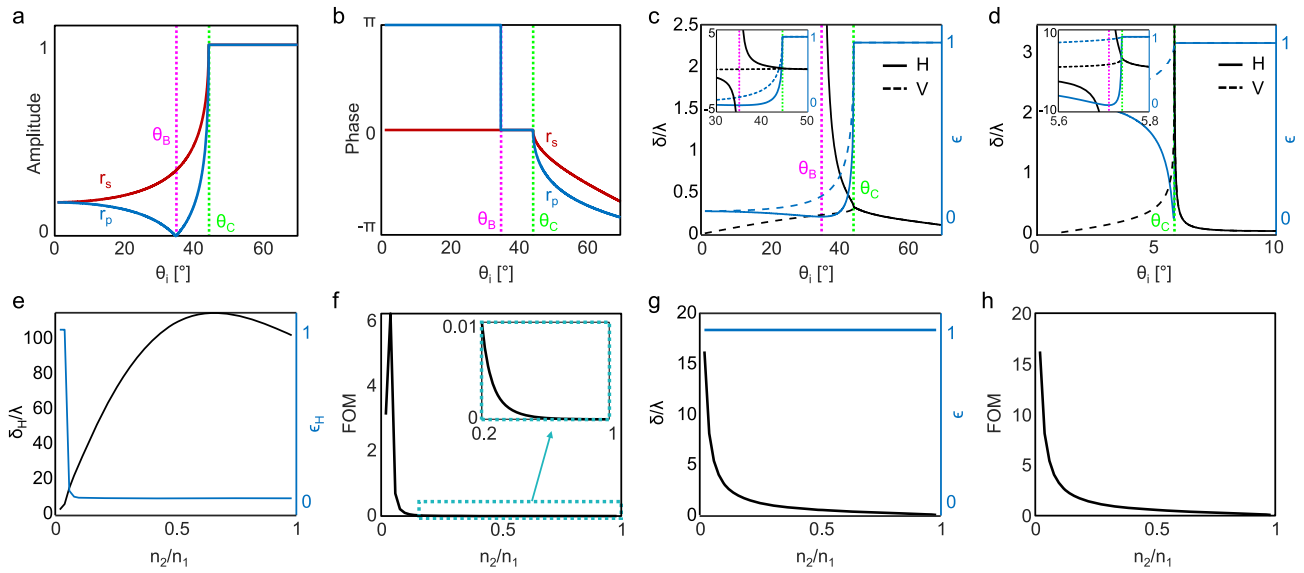

Figure 2. SHEL and its efficiency for a constant index contrast. Magenta and green lines correspond to θ_B and θ_C, respectively. (a) The amplitude and (b) phase of reflection coefficients when $n_2/n_1 = 0.7$. (c, d) δ/λ and ϵ when (c) $n_2/n_1 = 0.7$ and (d) $n_2/n_1 = 0.1$ for horizontal (solid) and vertical (dashed) polarizations. Insets show magnified views near θ_B and θ_C. (e) δ_H/λ, ϵ_H, and (f) FOM at $1.001\theta_B$. An inset shows a magnified view. (g) δ/λ, ϵ, and (h) FOM for both polarizations at θ_C.

This value corresponds to a theoretical maximum of the shift that is allowed to have a unity efficiency. At $\theta_i > \theta_C$, efficiencies remain unity, but the nonzero phase difference of r_s and r_p leads to the declination of the shift.

SHEL at a Critical Angle for a Constant Index Contrast. In this and the following section, we demonstrate that the large SHEL with unity efficiency can be achieved at a critical angle for a constant index and dispersion regimes respectively under both *s*- and *p*-polarized incidences. Then, generalization to the arbitrarily polarized incidence will be provided later. We first consider the simplest configuration, that is, an interface between two constant index media to investigate the SHEL while excluding other effects such as dispersive material properties. We examine r_s and r_p at an interface of a constant refractive index contrast $n_2/n_1 = 0.7$ (Figure 2a,b). Magenta and green dashed lines denote θ_B and θ_C, respectively. Two distinct features, zero reflection of *p* polarization and unity reflections of both polarizations, are observed at $\theta_i = \theta_B$ and $\theta_i > \theta_C$, respectively (Figure 2a). A phase difference between r_s and r_p is π at $\theta_i < \theta_B$, which is not favorable for achieving the large SHEL, and is ill-defined at θ_B due to the zero reflection (Figure 2b). Phase of r_p changes abruptly by π at θ_B and becomes equal to that of r_s at $\theta_B < \theta_i < \theta_C$. Both the amplitude and phase of r_s and r_p are equal at θ_C, while the phases deviate from each other as θ_i increases.

The SHEL and its efficiency can be directly calculated from the reflection coefficients according to eq 1. Although δ_H/λ increases remarkably near θ_B (black solid line, Figure 2c), ϵ_H is negligibly small in the corresponding range (blue solid line). In contrast, efficiencies become unity ($\epsilon_H = \epsilon_V = 1$) above θ_C as a result of total reflection. Because amplitudes of the two reflection coefficients are unity ($|r_s| = |r_p| = 1$), the shifts of two incident polarizations are also equal to each other ($\delta_H/\lambda = \delta_V/\lambda$) at $\theta_i > \theta_C$. Especially when $\theta_i = \theta_C$, the phase difference between two polarizations is zero, which is advantageous to obtain the large shift. A maximum value of δ/λ is achieved when $\epsilon = 1$ is 0.32 at θ_C for both polarizations, and this maximum value is only determined by θ_C (eq 3). A straightforward way to further enhance δ/λ is to increase the index contrast, that is, to reduce n_2/n_1. As n_2/n_1 becomes smaller, total reflection occurs at a smaller θ_i, and it leads to an increase of shift. The SHEL and its efficiency when $n_2/n_1 = 0.1$ are plotted in Figure 2d. The overall features are the same, but δ/λ at θ_C is significantly enhanced up to 3.18.

Note that the reflection coefficients are not differentiable with respect to θ_i at both θ_B and θ_C. This singularity may result in the failure of eq 1, especially when the beam waist is not large enough. Thus, the SHEL at $\theta_i = \theta_B$ and $\theta_i = \theta_C$ should be studied carefully. The shift calculated by using a wave packet model shows that eq 1 provides reasonable results except in an extremely narrow region of $|\theta_i - \theta_C| < 0.02°$ for $w_0 = 10\lambda$. The region in which eq 1 is invalid becomes narrower as w_0 increases and, thus, can be ignored for sufficiently large w_0 (see spin Hall effect of light at a singular incident angle, Supporting Information).

We define a figure-of-merit (FOM) as a magnitude of multiplication of the shift normalized by wavelength and efficiency: FOM = $\epsilon|\delta|/\lambda$. To examine the relation between the SHEL and the index contrast, δ/λ and ϵ are calculated along $1.001\theta_B$ and θ_C for various n_2/n_1 (Figure 2e–h). The slight deviation from θ_B is introduced to avoid singularities at θ_B. When n_2/n_1 is sufficiently small, θ_i exceeds θ_C and results in $\epsilon_H = 1$. However, ϵ_H drops down drastically in the remaining range. Therefore, despite the remarkable enhancement of δ_H/λ, near-zero ϵ_H leads to exceedingly small FOM (Figure 2e,f). In contrast, δ/λ and ϵ along θ_C exhibit entirely distinct characteristics (Figure 2g,h). In the whole parameter space, ϵ remains unity for both horizontal and vertical polarizations (Figure 2g). Meanwhile, δ/λ increases as n_2/n_1 decreases due to the decreasing θ_C. Because of the unity ϵ, FOM at θ_C is equal to the δ/λ and is much larger than that near θ_B (Figure 2h).

SHEL at a Critical Angle for a Dispersive Index Contrast. To see the relation between the SHEL and total reflection clearly, we examine an interface between air ($\varepsilon_1 = 1$) and a dispersive medium described by a Drude model $\varepsilon_2 = 2 -$

https://doi.org/10.1021/acsphotonics.1c00727
ACS Photonics XXXX, XXX, XXX−XXX

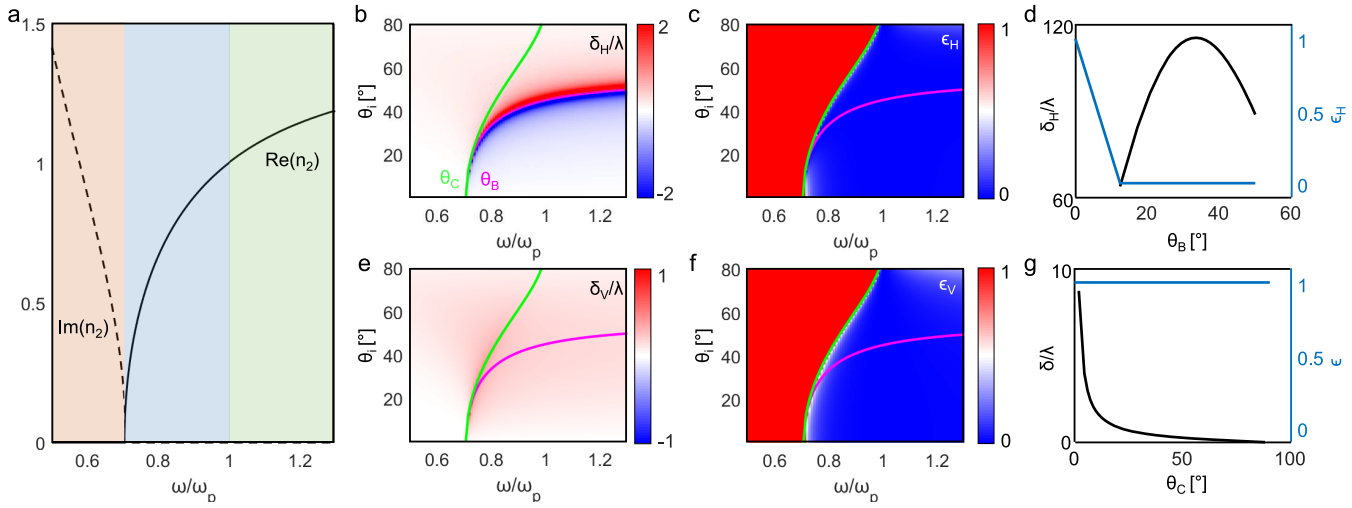

Figure 3. SHEL and its efficiency for a dispersive index contrast. (a) Index of the second medium. Permittivity is set as $\epsilon_1 = 1$, $\epsilon_2 = 2 - \omega_p^2/\omega^2$, where ω_p is a plasma frequency. Shaded areas with red, blue, and green denote metallic ($\mathrm{Re}(n_2) < 0$), low index ($0 < \mathrm{Re}(n_2) < 1$), and ordinary dielectric regime ($\mathrm{Re}(n_2) > 1$), respectively. (b) δ_H/λ and (c) ϵ_H for various frequencies and θ_i. (d) δ_H/λ and ϵ_H along $1.001\theta_B$. (e) δ_V/λ and (f) ϵ_V for various frequencies and θ_i. (g) δ/λ and ϵ for both polarizations along θ_C. Magenta and green lines correspond to θ_B and θ_C, respectively.

ω_p^2/ω^2, where ω_p is a plasma frequency (Figure 3a). We investigate a frequency range near ω_p to compare δ/λ and ϵ in three distinct regimes: metallic ($\mathrm{Re}(n_2) < 0$), low-index ($0 < \mathrm{Re}(n_2) < 1$), and ordinary dielectric ($\mathrm{Re}(n_2) > 1$) regimes, which are shaded as red, blue, and green, respectively. The SHEL and its efficiency for horizontal polarization in the whole parameter space are shown in Figure 3b,c. Here θ_B is defined only in the low-index and ordinary dielectric regimes. Along θ_B, δ_H/λ is significantly enhanced, yet ϵ_H is negligible (Figure 3d). Whereas the contribution of the total reflection to δ_H/λ is obscured by the strong enhancement along θ_B, especially when n_2 is close to zero, δ_V/λ shows the enhancement of the SHEL that originates solely from the total reflection (Figure 3e,f). Note that θ_C is defined only in the low-index regime. As n_2 converges to zero, δ_V/λ becomes drastically enhanced. The frequency bandwidth of the enhanced SHEL becomes narrow and is not clearly shown, hidden by the green curve in Figure 3e. Along θ_C, δ/λ has a maximum value while maintaining a unity efficiency (Figure 3g). This analysis is not restricted to a case in which the first medium is air, but can be applied to any interface that has the same ratio of indices (n_2/n_1).

SHEL under an Arbitrarily Polarized Source at a Critical Angle. Importantly, the SHEL with unity efficiency at θ_C not only works under horizontal and vertical polarizations but under any arbitrarily polarized incidence. In this section, we present a brief analytic proof of the incident-polarization-independent SHEL[40] at a critical angle. Circularly polarized components of the reflected beam can be expressed as

$$E_R^{\pm} = \frac{\omega_0}{2\sqrt{\pi}}[r_p \exp(\pm ik_y\Delta_H)E_I^H \pm ir_s \exp(\pm ik_y\Delta_V)E_I^V] \times \exp\left(-\frac{\omega_0^2(k_x^2 + k_y^2)}{4}\right) \quad (4)$$

where the subscripts I and R correspond to the incident and reflected beam respectively, $k_x \equiv k_{Ix} = -k_{Rx}$ and $k_y \equiv k_{Iy} = k_{Ry}$ are x- and y-components of the wave vector, and

$$\Delta_H = \frac{\cot\theta_i}{k_0}\left(1 + \frac{r_s}{r_p}\right), \quad \Delta_V = \frac{\cot\theta_i}{k_0}\left(1 + \frac{r_p}{r_s}\right) \quad (5)$$

where k_0 is the incident wave vector. Then, for an incidence with Jones vector $(E_I^H \quad E_I^V)$, the shift can be calculated as

$$\delta^{\pm} = \mathrm{Re}\frac{\langle E_R^{\pm}|i\partial_{k_y}|E_R^{\pm}\rangle}{\langle E_R^{\pm}|E_R^{\pm}\rangle} \quad (6)$$

If the two linear polarizations have the same reflection coefficients ($r_s = r_p$), $\Delta_H = \Delta_V$ and, hence, the expression in the square bracket in eq 4 are eigenstates of the operator $i\partial_{k_y}$ with eigenvalues $\mp\Delta$ for any $(E_I^H \quad E_I^V)$. Then $\delta^{\pm}$ depends on neither E_I^H nor E_I^V, but only on θ_i. To sum up, the SHEL has no polarization dependency and, therefore, the large SHEL with high efficiency occurs under any arbitrarily polarized incidence at a critical angle where $r_s = r_p = 1$.

Suggestion for Experimental Demonstration Using an Index-near-Zero Metamaterial. The easiest way to realize the large SHEL with a unity efficiency is to use total internal reflection at an interface between a dielectric medium and air, in which both the incident and the reflected beam are inside the dielectric medium. However, the SHEL that emerges in the dielectric medium is hard to be utilized and controlled in applications. Thus, it is sometimes preferable to use air as an incident medium. To realize total external reflection, a medium that has an index less than unity is required. Despite the many attempts to realize materials with unprecedented refractive indices, designs proposed so far as epsilon-near-zero or index-below-unity metamaterials operate in limited conditions such as for a specific polarization.[41−48] The polarization dependency originates from an anisotropic geometry of the metal−dielectric multilayer.[41,42]

Here we suggest the design of a 3D isotropic index-near-zero metamaterial for experimental confirmation. A unit structure consists of three orthogonal interconnecting metallic wires

https://doi.org/10.1021/acsphotonics.1c00727
ACS Photonics XXXX, XXX, XXX−XXX

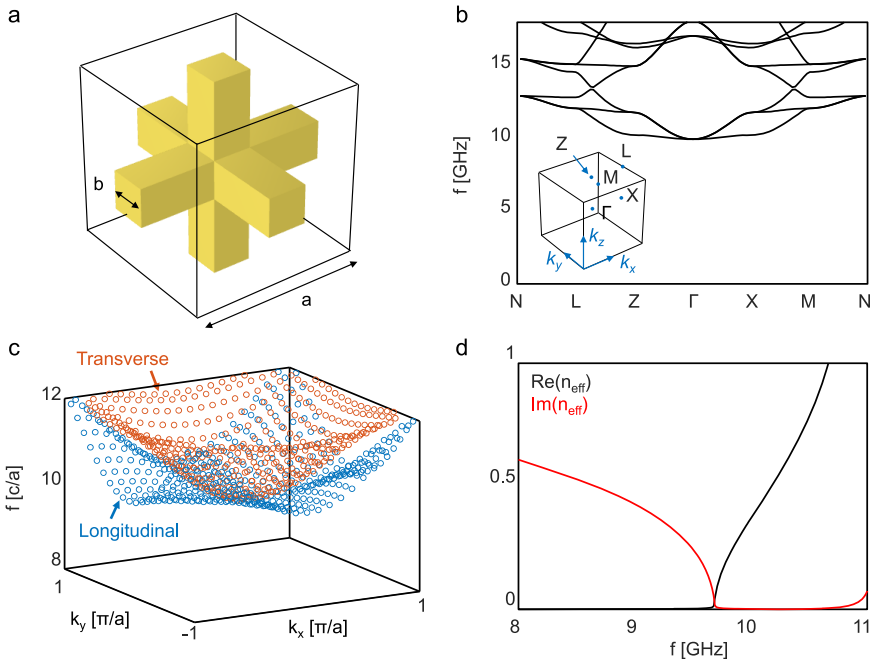

Figure 4. 3D isotropic index-near-zero metamaterial and its optical properties. (a) A unit cell of the 3D wire medium. The metallic part is represented as yellow. Geometrical parameters a and b correspond to the lattice constant and the wire width, respectively. (b) Band structure when $b = 0.3a$. Inset shows the first Brillouin zone with high symmetry points. (c) Band structure of two lowest modes in a k_x–k_y plane ($k_z = 0$). Blue and red markers denote longitudinal and transverse modes, respectively. (d) Effective index extracted by using the S-parameter retrieval method.

presented in ref 49 (Figure 4a). This structure operating in a microwave regime can be fabricated by using a binder jetting method.[50] The wire is considered as a perfect electrical conductor, and the background medium is air ($n = 1$). Band structure of the 3D wire medium with geometric parameters a = 15.9 mm and $b = 0.3a$ has a bandgap below a cutoff frequency 9.93 GHz (Figure 4b) (see band structures of the 3D wire medium for various wire widths, Supporting Information). Above the cutoff frequency are two eigenmodes, one longitudinal and the other transverse mode (Figure 4c). Equifrequency contours of these eigenmodes are points, which correspond to zero index, at the cutoff frequency. The contours become two concentric circles that have slightly different radii right above the cutoff. Thus, the 3D wire medium is expected to behave as a metal in the bandgap regime, as a zero-index-material at the cutoff frequency, and as an index-below-unity material slightly above the cutoff.

To quantitatively prove that the 3D wire medium indeed satisfies such properties, the effective index $n_{eff} = \sqrt{\varepsilon_{eff}}$ is retrieved from S-parameters,[51] where

$$\varepsilon_{eff} = \frac{2}{ik_0 d}\frac{s^{++} + s^{-+} - 1}{s^{++} + s^{-+} + 1} \tag{7}$$

Here s is the S-parameter, the first and second superscripts of which represent propagation directions of the transmitted and incident beams, respectively (+ for forward and − for backward), and d is the thickness of the wire medium used for simulation. Figure 4d shows n_{eff} near the cutoff frequency. The 3D wire medium has metallic properties, characterized by $\mathrm{Re}(n_{eff}) = 0$ and $\mathrm{Im}(n_{eff}) > 0$, below the cutoff and has low index properties, manifested by $0 < \mathrm{Re}(n_{eff}) < 1$ and $\mathrm{Im}(n_{eff}) = 0$, above the cutoff. The SHEL at boundaries of the 3D wire medium can be confirmed experimentally using horn antenna measurements in the microwave (see experimental demonstration in the microwave regime, Supporting Information).

Lastly, we address two limitations of this index-near-zero metamaterial for completeness. First, the operating frequency is constrained to a narrow regime above the cutoff frequency. This narrow bandwidth is also associated with narrow bounds centered at the origin (Γ-point) in momentum space. Thus, the index-near-zero properties only appear under near-normal incidence, that is, under a small θ_i. This narrow bandwidth is, however, a universal limitation of zero-index or index-near-zero metamaterials. Second, the fabrication of such a 3D structure operating in optical frequencies is not straightforward because of the difficulties in electroplating the horizontal wires. Nevertheless, the large SHEL along with near-unity efficiency can be achieved by the total external reflection occurring at boundaries of such a judiciously designed index-near-zero metamaterial.

DISCUSSIONS AND CONCLUSION

There exist several naturally available or specially prepared materials that have an index less than unity in other frequency regimes. Possible candidates include naturally available materials such as metals in the ultraviolet,[52] heavily doped semiconductors in the terahertz,[53] and inorganic compounds in the mid-infrared regime.[54,55] A random mixture of two natural materials such as a dielectric with subwavelength metallic inclusions can also have an index below unity in the visible. The large SHEL can be achieved with high efficiency using such materials in the optical regime by carefully designing the index-near-zero metamaterials to have low loss.[56] It is worth to note that our approach should be applied carefully if the index-near-zero materials are lossy. Total external reflection cannot occur in the presence of losses as a consequence of partial absorption. Therefore, the SHEL and its efficiency decrease as the ratio of losses of two media increases

https://doi.org/10.1021/acsphotonics.1c00727
ACS Photonics XXXX, XXX, XXX−XXX

(see spin Hall effect of light at an interface of lossy medium, Supporting Information).

The required condition of the total external reflection, that is, a lossless and isotropic medium that has an index less than unity, can be relaxed to a low symmetry case, that is, an anisotropic case. If the effective index perpendicular to the incident plane (n_s) is below unity, then an *s*-polarized incidence, which is decoupled to the refractive indices along the other directions, still undergoes total external reflection at $\theta_i = \sin^{-1}(n_s/n_1)$. In such a case, the SHEL has a unity efficiency under *s*-polarization ($\epsilon_V = 1$). However, δ_V/λ cannot reach the theoretical maximum (eq 3) because $r_s = r_p$ is not satisfied. On the other hand, *p*-polarized incidence undergoes a partial reflection, which leads to degradation of both δ_V/λ and ϵ_V. To sum up, the large SHEL with unity efficiency is also possible for vertically polarized incidence in a low symmetric case where only refractive index along the transverse axis is less than unity. The SHEL with a unity efficiency for *s* polarization should be clearly distinguished from our previous work based on the anisotropic impedance mismatching,[39] in which near-unity reflection originates from metallic properties rather than index less than unity.

In conclusion, we present a new approach based on total reflection to achieve the large SHEL and unity efficiency simultaneously. A beam reflected at an interface of dense-to-sparse medium exhibits the SHEL with unity efficiency and a shift that reaches a theoretical maximum at a critical angle. We also suggest a design of a 3D isotropic index-near-zero metamaterial, boundaries of which act as an interface for total external reflection, as a platform to experimentally verify the SHEL with high efficiency. The sharp enhancement of the SHEL along with high efficiency at a critical angle can be useful in spin-dependent photonic devices such as switches and filters.

METHOD

Numerical Simulation. Band structure and reflection coefficients of the 3D wire medium were calculated by a finite element method-based commercial software (COMSOL Multiphysics 5.5). For the band structure, a unit cell with periodic boundary conditions along all boundaries was simulated using an eigenfrequency solver. For reflection coefficients, ten layers of unit cell aligned along the *z*-axis were used with air as a background medium. Bloch boundary conditions were applied along the *x*- and *y*-normal boundaries.

ASSOCIATED CONTENT

Supporting Information

The Supporting Information is available free of charge at https://pubs.acs.org/doi/10.1021/acsphotonics.1c00727.

Spin Hall effect of light at a singular incident angle, band structures of the 3D wire medium for various wire widths, experimental demonstration in the microwave regime, and spin Hall effect of light at an interface of lossy media (PDF)

AUTHOR INFORMATION

Corresponding Author

Junsuk Rho − *Department of Mechanical Engineering and Department of Chemical Engineering, Pohang University of Science and Technology (POSTECH), Pohang 37673, Republic of Korea; POSCO-POSTECH-RIST Convergence Research Center for Flat Optics and Metaphotonics, Pohang 37673, Republic of Korea;* orcid.org/0000-0002-2179-2890; Email: jsrho@postech.ac.kr

Authors

Minkyung Kim − *Department of Mechanical Engineering, Pohang University of Science and Technology (POSTECH), Pohang 37673, Republic of Korea*

Dasol Lee − *Department of Mechanical Engineering, Pohang University of Science and Technology (POSTECH), Pohang 37673, Republic of Korea; Department of Biomedical Engineering, Yonsei University, Wonju 26493, Republic of Korea*

Thi Hai-Yen Nguyen − *Department of Electrical Engineering, Ulsan National Institute of Science and Technology (UNIST), Ulsan 44919, Republic of Korea*

Hee-Jo Lee − *Department of Physics Education, Deagu University, Gyeongsan 38453, Republic of Korea*

Gangil Byun − *Department of Electrical Engineering, Ulsan National Institute of Science and Technology (UNIST), Ulsan 44919, Republic of Korea*

Complete contact information is available at: https://pubs.acs.org/10.1021/acsphotonics.1c00727

Author Contributions

#These authors contributed equally to this work.

Notes

The authors declare no competing financial interest.

ACKNOWLEDGMENTS

This work was financially supported by the POSCO-POSTECH-RIST Convergence Research Center program funded by POSCO, and the National Research Foundation (NRF) Grants (NRF-2019R1A2C3003129, CAMM-2019M3A6B3030637, NRF-2019R1A5A8080290) funded by the Ministry of Science and ICT of the Korean government. M.K. acknowledges the NRF Global Ph.D. Fellowship (NRF-2017H1A2A1043204) funded by the Ministry of Education of the Korean government.

REFERENCES

(1) Born, M.; Wolf, E. *Principles of optics: electromagnetic theory of propagation, interference and diffraction of light*; Cambridge University Press, 2013.

(2) Bliokh, K. Y.; Rodríguez-Fortuño, F. J.; Nori, F.; Zayats, A. V. Spin−orbit interactions of light. *Nat. Photonics* **2015**, *9*, 796−808.

(3) Bokor, N.; Iketaki, Y.; Watanabe, T.; Fujii, M. Investigation of polarization effects for high-numerical-aperture first-order Laguerre-Gaussian beams by 2D scanning with a single fluorescent microbead. *Opt. Express* **2005**, *13*, 10440−10447.

(4) Darsht, M. Y.; Zel'Dovich, B. Y.; Kataevskaya, I. V.; Kundikova, N. Formation of an isolated wavefront dislocation. *J. Exp. Theor. Phys.* **1995**, *80*, 817−821.

(5) Bekshaev, A. Y.; Bliokh, K. Y.; Nori, F. Transverse Spin and Momentum in Two-Wave Interference. *Phys. Rev. X* **2015**, *5*, 011039.

(6) Xiao, S.; Zhong, F.; Liu, H.; Zhu, S.; Li, J. Flexible coherent control of plasmonic spin-Hall effect. *Nat. Commun.* **2015**, *6*, 8360.

(7) Onoda, M.; Murakami, S.; Nagaosa, N. Hall effect of light. *Phys. Rev. Lett.* **2004**, *93*, 083901.

(8) Hosten, O.; Kwiat, P. Observation of the spin Hall effect of light via weak measurements. *Science* **2008**, *319*, 787−790.

(9) Bliokh, K. Y.; Samlan, C. T.; Prajapati, C.; Puentes, G.; Viswanathan, N. K.; Nori, F. Spin-Hall effect and circular birefringence of a uniaxial crystal plate. *Optica* **2016**, *3*, 1039−1047.

(10) Ling, X.; Zhou, X.; Huang, K.; Liu, Y.; Qiu, C.-W.; Luo, H.; Wen, S. Recent advances in the spin Hall effect of light. *Rep. Prog. Phys.* **2017**, *80*, 066401.
(11) Xiao, S.; Wang, J.; Liu, F.; Zhang, S.; Yin, X.; Li, J. Spin-dependent optics with metasurfaces. *Nanophotonics* **2017**, *6*, 215−234.
(12) Ling, X.; Guan, F.; Cai, X.; Ma, S.; Xu, H.-X.; He, Q.; Xiao, S.; Zhou, L. Topology-Induced Phase Transitions in Spin-Orbit Photonics. *Laser Photonics Rev.* **2021**, *15*, 2000492.
(13) Qin, Y.; Li, Y.; He, H.; Gong, Q. Measurement of spin Hall effect of reflected light. *Opt. Lett.* **2009**, *34*, 2551−2553.
(14) Wang, B.; Rong, K.; Maguid, E.; Kleiner, V.; Hasman, E. Probing nanoscale fluctuation of ferromagnetic meta-atoms with a stochastic photonic spin Hall effect. *Nat. Nanotechnol.* **2020**, *15*, 450−456.
(15) Chen, S.; Ling, X.; Shu, W.; Luo, H.; Wen, S. Precision Measurement of the Optical Conductivity of Atomically Thin Crystals via the Photonic Spin Hall Effect. *Phys. Rev. Appl.* **2020**, *13*, 014057.
(16) Li, T.; Wang, Q.; Taallah, A.; Zhang, S.; Yu, T.; Zhang, Z. Measurement of the magnetic properties of thin films based on the spin Hall effect of light. *Opt. Express* **2020**, *28*, 29086−29097.
(17) Qiu, X.; Zhou, X.; Hu, D.; Du, J.; Gao, F.; Zhang, Z.; Luo, H. Determination of magneto-optical constant of Fe films with weak measurements. *Appl. Phys. Lett.* **2014**, *105*, 131111.
(18) Liu, J.; Zeng, K.; Xu, W.; Chen, S.; Luo, H.; Wen, S. Ultrasensitive detection of ion concentration based on photonic spin Hall effect. *Appl. Phys. Lett.* **2019**, *115*, 251102.
(19) Zhou, X.; Ling, X.; Luo, H.; Wen, S. Identifying graphene layers via spin Hall effect of light. *Appl. Phys. Lett.* **2012**, *101*, 251602.
(20) Wang, R.; Zhou, J.; Zeng, K.; Chen, S.; Ling, X.; Shu, W.; Luo, H.; Wen, S. Ultrasensitive and real-time detection of chemical reaction rate based on the photonic spin Hall effect. *APL Photonics* **2020**, *5*, 016105.
(21) Zhou, X.; Xiao, Z.; Luo, H.; Wen, S. Experimental observation of the spin Hall effect of light on a nanometal film via weak measurements. *Phys. Rev. A* **2012**, *85*, 043809.
(22) Yang, Y.; Lee, T.; Kim, M.; Jung, C.; Badloe, T.; Lee, D.; Lee, S.; Lee, H.-J.; Rho, J. Dynamic optical spin Hall effect in chitosan-coated all-dielectric metamaterials for a biosensing platform. *IEEE J. Sel. Top. Quantum Electron.* **2021**, *27*, 7300608.
(23) Bliokh, K. Y.; Prajapati, C.; Samlan, C. T.; Viswanathan, N. K.; Nori, F. Spin-Hall effect of light at a tilted polarizer. *Opt. Lett.* **2019**, *44*, 4781−4784.
(24) Mazanov, M.; Yermakov, O.; Deriy, I.; Takayama, O.; Bogdanov, A.; Lavrinenko, A. V. Photonic Spin Hall Effect: Contribution of Polarization Mixing Caused by Anisotropy. *Quantum Reports* **2020**, *2*, 489−500.
(25) Takayama, O.; Puentes, G. Enhanced spin Hall effect of light by transmission in a polymer. *Opt. Lett.* **2018**, *43*, 1343−1346.
(26) Tang, T.; Zhang, Y.; Li, J.; Luo, L. Spin Hall Effect Enhancement of Transmitted Light Through an Anisotropic Metamaterial Slab. *IEEE Photonics J.* **2017**, *9*, 4600910.
(27) Tang, T.; Li, C.; Luo, L. Enhanced spin Hall effect of tunneling light in hyperbolic metamaterial waveguide. *Sci. Rep.* **2016**, *6*, 30762.
(28) Takayama, O.; Sukham, J.; Malureanu, R.; Lavrinenko, A. V.; Puentes, G. Photonic spin Hall effect in hyperbolic metamaterials at visible wavelengths. *Opt. Lett.* **2018**, *43*, 4602−4605.
(29) Kim, M.; Lee, D.; Kim, T. H.; Yang, Y.; Park, H. J.; Rho, J. Observation of enhanced optical spin Hall effect in a vertical hyperbolic metamaterial. *ACS Photonics* **2019**, *6*, 2530−2536.
(30) Zhu, W.; She, W. Enhanced spin Hall effect of transmitted light through a thin epsilon-near-zero slab. *Opt. Lett.* **2015**, *40*, 2961−2964.
(31) Jiang, X.; Tang, J.; Li, Z.; Liao, Y.; Jiang, L.; Dai, X.; Xiang, Y. Enhancement of photonic spin Hall effect via bound states in the continuum. *J. Phys. D: Appl. Phys.* **2019**, *52*, 045401.
(32) Yin, X.; Ye, Z.; Rho, J.; Wang, Y.; Zhang, X. Photonic spin Hall effect at metasurfaces. *Science* **2013**, *339*, 1405−1407.
(33) Götte, J. B.; Löffler, W.; Dennis, M. R. Eigenpolarizations for Giant Transverse Optical Beam Shifts. *Phys. Rev. Lett.* **2014**, *112*, 233901.
(34) Qiu, X.; Zhang, Z.; Xie, L.; Qiu, J.; Gao, F.; Du, J. Incident-polarization-sensitive and large in-plane-photonic-spin-splitting at the Brewster angle. *Opt. Lett.* **2015**, *40*, 1018−1021.
(35) Luo, H.; Zhou, X.; Shu, W.; Wen, S.; Fan, D. Enhanced and switchable spin Hall effect of light near the Brewster angle on reflection. *Phys. Rev. A* **2011**, *84*, 043806.
(36) Dai, H.; Yuan, L.; Yin, C.; Cao, Z.; Chen, X. Direct Visualizing the Spin Hall Effect of Light via Ultrahigh-Order Modes. *Phys. Rev. Lett.* **2020**, *124*, 053902.
(37) Kim, M.; Lee, D.; Ko, B.; Rho, J. Diffraction-induced enhancement of optical spin Hall effect in a dielectric grating. *APL Photonics* **2020**, *5*, 066106.
(38) Zhou, X.; Ling, X. Enhanced Photonic Spin Hall Effect Due to Surface Plasmon Resonance. *IEEE Photonics J.* **2016**, *8*, 4801108.
(39) Kim, M.; Lee, D.; Cho, H.; Min, B.; Rho, J. Spin Hall Effect of Light with Near-Unity Efficiency in the Microwave. *Laser Photonics Rev.* **2021**, *15*, 2000393.
(40) Kim, M.; Lee, D.; Rho, J. Spin Hall Effect under Arbitrarily Polarized or Unpolarized Light. *Laser Photonics Rev.* **2021**, *15*, 2100138.
(41) Maas, R.; Parsons, J.; Engheta, N.; Polman, A. Experimental realization of an epsilon-near-zero metamaterial at visible wavelengths. *Nat. Photonics* **2013**, *7*, 907−912.
(42) Subramania, G.; Fischer, A.; Luk, T. Optical properties of metal-dielectric based epsilon near zero metamaterials. *Appl. Phys. Lett.* **2012**, *101*, 241107.
(43) Gao, J.; Sun, L.; Deng, H.; Mathai, C. J.; Gangopadhyay, S.; Yang, X. Experimental realization of epsilon-near-zero metamaterial slabs with metal-dielectric multilayers. *Appl. Phys. Lett.* **2013**, *103*, 051111.
(44) Li, Y.; Kita, S.; Muñoz, P.; Reshef, O.; Vulis, D. I.; Yin, M.; Lončar, M.; Mazur, E. On-chip zero-index metamaterials. *Nat. Photonics* **2015**, *9*, 738−742.
(45) Liberal, I.; Engheta, N. Near-zero refractive index photonics. *Nat. Photonics* **2017**, *11*, 149−158.
(46) Schwartz, B.; Piestun, R.; Boulder, A. A new path: Ultra-low index metamaterials present new possibilities for controlling light propagation. *SPIE's oemagazine* **2005**, 30−32.
(47) Schwartz, B. T.; Piestun, R. Total external reflection from metamaterials with ultralow refractive index. *J. Opt. Soc. Am. B* **2003**, *20*, 2448−2453.
(48) Schwartz, B. T.; Piestun, R. Waveguiding in air by total external reflection from ultralow index metamaterials. *Appl. Phys. Lett.* **2004**, *85*, 1.
(49) Chen, W.-J.; Hou, B.; Zhang, Z.-Q.; Pendry, J. B.; Chan, C.-T. Metamaterials with index ellipsoids at arbitrary k-points. *Nat. Commun.* **2018**, *9*, 2086.
(50) Ziaee, M.; Crane, N. B. Binder jetting: A review of process, materials, and methods. *Addit. Manuf.* **2019**, *28*, 781−801.
(51) Feng, T.; Liu, F.; Tam, W. Y.; Li, J. Effective parameters retrieval for complex metamaterials with low symmetries. *EPL (Europhysics Letters)* **2013**, *102*, 18003.
(52) Whang, U. S.; Arakawa, E. T.; Callcott, T. A. Optical Properties of K between 4 and 10.7 eV and Comparison with Na, Rb, and Cs. *Phys. Rev. B* **1972**, *6*, 2109.
(53) Nashima, S.; Morikawa, O.; Takata, K.; Hangyo, M. Measurement of optical properties of highly doped silicon by terahertz time domain reflection spectroscopy. *Appl. Phys. Lett.* **2001**, *79*, 3923.
(54) Kischkat, J.; Peters, S.; Gruska, B.; Semtsiv, M.; Chashnikova, M.; Klinkmüller, M.; Fedosenko, O.; Machulik, S.; Aleksandrova, A.; Monastyrskyi, G.; Flores, Y.; Masselink, W. T. Mid-infrared optical properties of thin films of aluminum oxide, titanium dioxide, silicon dioxide, aluminum nitride, and silicon nitride. *Appl. Opt.* **2012**, *51*, 6789−6798.

https://doi.org/10.1021/acsphotonics.1c00727
ACS Photonics XXXX, XXX, XXX−XXX

(55) Querry, M. *Optical Constants, Contractor Report*; U.S. Army Chemical Research, Development and Engineering Center (CRDC): Aberdeen Proving Ground, MD, 1985; Vol. *418*.
(56) Dong, T.; Liang, J.; Camayd-Munoz, S.; Liu, Y.; Tang, H.; Kita, S.; Chen, P.; Wu, X.; Chu, W.; Mazur, E.; Li, Y. Ultra-low-loss on-chip zero-index materials. *Light: Sci. Appl.* **2021**, *10*, 10.

https://doi.org/10.1021/acsphotonics.1c00727
ACS Photonics XXXX, XXX, XXX−XXX